Published in final edited form as:
Mitochondrion. 2010 March ; 10(2): 125–136. doi:10.1016/j.mito.2009.11.003.

Mitochondrial respiratory chain dysfunction variably increases oxidant stress in *Caenorhabditis elegans*

Stephen Dingley[1], **Erzsebet Polyak**[1], **Richard Lightfoot**[2], **Julian Ostrovsky**[1], **Meera Rao**[1], **Todd Greco**[2], **Harry Ischiropoulos**[2], and **Marni J. Falk**[1,*]

Stephen Dingley: stephen.dingley@gmail.com; Erzsebet Polyak: polyake@email.chop.edu; Richard Lightfoot: lightfoot@email.chop.edu; Julian Ostrovsky: ostrovskyj@email.chop.edu; Meera Rao: meerao@sas.upenn.edu; Todd Greco: tgreco@mail.med.upenn.edu; Harry Ischiropoulos: ischirop@mail.med.upenn.edu

[1]Division of Human Genetics, Department of Pediatrics, The Children's Hospital of Philadelphia and University of Pennsylvania, Philadelphia, PA 19104, USA

[2]Division of Neonatology, Department of Pediatrics, The Children's Hospital of Philadelphia and University of Pennsylvania, Philadelphia, PA 19104, USA

Abstract

Mitochondrial dysfunction and associated oxidant stress have been linked with numerous complex diseases and aging largely by *in vitro* determination of mitochondria oxidant production and scavenging. We applied targeted *in vivo* fluorescence analyses of mitochondria-dense pharyngeal tissue in *C. elegans* to better understand relative mitochondrial effects, particularly on matrix oxidant burden, of respiratory chain complex, MnSOD, and insulin receptor mutants displaying variable longevity. The data demonstrate significantly elevated *in vivo* matrix oxidant burden in the short-lived complex I mutant, *gas-1*(*fc21*), which was associated with limited superoxide scavenging capacity despite robust MnSOD induction, as well as decreased mitochondria content and membrane potential. Significantly increased MnSOD activity was associated with *in vivo* matrix oxidant levels similar to wild-type in the long-lived respiratory chain complex III mutant, *isp-1*(*qm150*). Yet, despite greater superoxide scavenging capacity in the complex III mutant than in the significantly longer-lived insulin receptor mutant, *daf-2*(*e1368*), only the former showed modest oxidative stress sensitivity. Furthermore, increased longevity was seen in MnSOD knockout mutants (*sod-2*(*ok1030*) *and sod-2*(*gk257*)) that had decreased MnSOD scavenging capacity and increased *in vivo* matrix oxidant burden. Thus, factors beside oxidant stress must underlie RC mutant longevity in *C. elegans*. This work highlights the utility of the *C. elegans* model as a tractable means to non-invasively monitor multi-dimensional *in vivo* consequences of primary mitochondrial dysfunction.

Keywords

Complexes I, II, and III; MnSOD; membrane potential; MitoSOX; TMRE; fluorescence microscopy

*Corresponding Author: Marni J. Falk, MD, ARC 1002c, 3615 Civic Center Blvd, Philadelphia, PA 19104, office 215-590-4564; fax 267-426-2876, falkm@email.chop.edu.

1. INTRODUCTION

Oxidative stress resulting from increased production of reactive species and/or concomitant decline in antioxidant scavenging capacity may damage proteins, lipids, nucleic acids and other cellular structures (Valko et al. 2006). Such multi-faceted cellular damage may contribute to many sporadic (Schapira 2006) and inherited (DiMauro 2004) mitochondrial diseases and aging (Rea et al. 2007). Up to 2% of total oxygen consumed by the mitochondrial respiratory chain (RC) in *in vitro* studies, and 0.2% under more physiologic conditions (Balaban et al. 2005), has been shown to be improperly reduced to generate superoxide, which is then released into the matrix primarily from complex I (Murphy 2009) or intermembrane space exclusively from complex III (Chen et al. 2003; Murphy 2009). Superoxide dismutase (SOD) offers a primary oxidant defense through rapid conversion of superoxide radicals into hydrogen peroxide and oxygen. Three human SOD genes localize to different subcellular compartments, where *SOD2* encodes the manganese SOD that functions within the mitochondria matrix.

Assessing the relative balance of oxidant production and scavenging *in vivo* remains a significant challenge (Yang et al. 2007). The development of small, lipophilic molecules that emit fluorescence only in the oxidized form has permitted a method of semi-quantitative evaluation of oxidant burden in cellular model systems. In particular, mitochondria-specific oxidant levels can be assessed using the fluorescent probe, MitoSOX Red, a lipophilic hydroethidine (HE) derivative that accumulates 100- to 1000-fold within mitochondria due to charge attraction of its triphenylphosphonium cation through the mitochondria membrane bilayers into the negatively-charged mitochondria matrix (Robinson et al. 2008). Mitochondria-generated oxidants react with MitoSOX to yield two primary fluorescent products, a 2-hydroxyethidium derivative (2-OH-Mito-E^+) resulting from superoxide oxidation, and Mito-E^+, a non-specific oxidized product (Zielonka et al. 2008). Reliable interpretation of fluorescence analyses that rely upon mitochondria membrane potential (DeltaPsi(m) or $\Delta\Psi_m$) for dye distribution may be subject to diminished or enhanced dye uptake, although several fluorescent dyes are now commonly used for *in vitro* $\Delta\Psi_m$ assessment (O'Reilly et al. 2003). Membrane potential indicator dyes have recently been applied *in vivo* in the model animal, *C. elegans* (Gaskova et al. 2007; Zuryn et al. 2008).

C. elegans offers a facile model in which to study a host of *in vivo* mitochondria functions. Nematodes incorporate ingested fluorescent dyes into their cells and are optically transparent, which permits precise assessment of tissue and cellular dye localization. Furthermore, several well-characterized *C. elegans* strains harboring mutations in nuclear genes encoding mitochondrial proteins are easily accessible (www.wormbase.org). However, assessing mitochondria functions by quantitative analysis of whole animal fluorescence may be limited by non-specific binding of lipophilic, fluorescence-based reagents, particularly within the lipid-rich granules of the gastrointestinal tract (Clokey and Jacobson 1986). Thus, we sought to identify *C. elegans* tissues having high metabolic activity that might offer a focus for the further study of mitochondria physiology. *C. elegans* actively transports and grinds food (i.e., bacteria) between its mouth and intestines through a muscle-tube like pharynx, which consists largely of anterior and terminal pharyngeal bulbs (PB) joined by an isthmus (Altun and Hall 2008). The pharynx shares several similarities with the mammalian heart including near-continuous and intrinsic myogenic electrical activity (up to 250 beats per minute) (Avery and Horvitz 1989), electrical coupling between muscle cells (Starich et al. 1996), calcium-based action potentials (Shtonda and Avery 2005), and high mitochondria density (Altun and Hall 2008). Capitalizing on these anatomical features and the existence of well-characterized *C. elegans* mutants, we evaluated the relative *in vivo* mitochondria oxidant production and mitochondria membrane potential ($\Delta\Psi_m$) in RC and insulin receptor mutants displaying variable longevity, as well as

in MnSOD mutants with primary impairment of mitochondria superoxide scavenging capacity. We demonstrate that *C. elegans* offers a powerful model in which to assess the *in vivo*, multi-dimensional consequences of mitochondrial dysfunction, as well as to explore the complex relationship between oxidant stress and longevity under varying genetic and environmental conditions.

2. METHODS

2.1 Strains growth and maintenance

C. elegans worm strains were obtained from the *Caenorhabditis* Genetics Center (University of Minnesota, Minneapolis, MN) (Table 1). Strains studied included wild-type (N2 Bristol), three mitochondrial RC mutants in complexes I, II, and III [*gas-1(fc21), mev-1(kn1), isp-1(qm150),* respectively], and the insulin receptor mutant *(daf-2 (e1368)).* All superoxide scavenging (MnSOD) mutant strains studied harbored loss-of-function mutations, including two *sod-2* alleles [*sod-2(gk257)* is homozygous for a complex mutation characterized by an 18 basepair insertion and 159 basepair deletion; *sod-2(ok1030)* has a 900 basepair homozygous deletion] and a single allele of *sod-3* [*sod-3(gk235)* is homozygous for a complex rearrangement characterized by a 6 basepair insertion and 390 basepair deletion] (www.wormbase.org). Nematodes were grown at 20°C on nematode growth media (NGM) plates spread with OP50 *E. coli*. For all fluorescent studies, synchronous young adult populations were obtained by bleaching gravid adults on NGM plates (Hope 1999), plating the recovered eggs onto unspread NGM plates overnight, and then transferring L1-arrested animals the next day to NGM plates spread with OP50 *E. coli*. Upon reaching adulthood (defined by the presence of eggs laid on the plate), nematodes were washed off in S. basal (3.4 g KH_2PO_4, 4.4 g K_2HPO_4, 5.85 g NaCl, 1 liter water, pH 7.0) and adults were separated from eggs by gravity. For mass spectrometry study of whole worm aliquots (see below) as well as for mitochondria isolation, nematodes were grown at 20°C on 20 large NGM plates spread with OP50 *E. coli* for two generations, and then grown in 1 liter liquid culture flasks with K12 *E. coli* at 200 rpm in shaking 20°C incubators (I26/R Series, New Brunswick Scientific, Edison, NJ). Worms were harvested from liquid culture, as previously described (Falk 2006, Hope 1999).

2.2 Lifespan assessment

Animals were maintained at 20°C throughout the experiment. Synchronized nematode cultures were initiated by bleaching young adults to obtain eggs. Collected eggs were allowed to hatch overnight on 10 cm unspread NGM plates, after which L1-arrested larvae were transferred to 10 cm NGM plates spread with OP50 *E. coli*. Upon reaching the first day of egg laying, synchronous young adults were moved to fresh 3.5 cm NGM plates seeded with OP50 *E. coli* (lifespan experiment “Day 0”). For purposes of higher-throughput lifespan screening by preventing offspring from nematodes under study from reaching adulthood, fluorodeoxyuridine (FUDR) was added to OP50-spread NGM plates to a final concentration of 100 *u*g/ml (Hamilton et al. 2005). 40 to 60 nematodes were studied per strain, divided on two 3.5 cm NGM plates. Mortality was confirmed by stimulating nematodes lightly with a platinum wire; nematodes that did not move after stimulation were scored as dead and removed from the plate. Worms that died of protruding/bursting vulva, bagging, or crawling off the agar were censored. All lifespan studies were performed by a single technician (J.O.). Median, mean, and maximal lifespan were determined for each strain relative to concurrently studied wild-type worms.

2.3 Relative quantitation of mitochondria superoxide levels by fluorescence microscopy

All fluorescent studies were performed at 20°C in dim light. An initial time course experiment was carried out in wild-type (N2 Bristol) worms to assess the optimal duration

of dye exposure in living animals. Terminal PB mean fluorescence intensity was determined in synchronous young adult nematodes following 12, 36, and 60 hours of 10 *u*M MitoSOX exposure with or without paraquat (either at a low dose of 200 *u*M or a high dose of 20 mM). The relative contribution of *E. coli* to observed fluorescence was assessed through comparison of nematodes fed OP50 that was live or killed by UV exposure for 30 minutes. Fluorescence microscopy analysis and quantitation was performed on an Olympus IX70 fluorescence microscope with a HQ500/30x Q530LP HQ610/75m cube set (CHROMA Technology Group, Rockingham, VT), using the Metamorph image acquisition and analysis software package (Molecular Devices Corp, Downingtown, PA). Two additional time-course experiments were subsequently performed in N2 Bristol nematodes fed 10 *u*M MitoSOX Red using the same microscope and software detailed below to confirm that similar peak fluorescence occur following 24 hour exposures regardless of analysis platform.

Synchronous young adult stage worm populations of each strain were grown on NGM plates spread with OP50 *E. coli* and either 10 *u*M MitoSOX Red (Molecular Probes, Eugene, OR) alone or with 1 mM paraquat (Sigma, St. Louis, MO) to induce oxidant stress (Bus and Gibson 1984; Cocheme and Murphy 2009). Following 24-hour incubation, nematodes were transferred to fresh NGM plates spread with OP50 *E. coli* for one hour to clear their guts of residual dye. Living nematodes were paralyzed *in situ* by directly adding 1 mg/ml levamisole to NGM agar plates. Photographs were taken immediately in a dark room at 160X magnification and 2 second exposure time using a CY3 fluorescence cube set (MZFLIII, Leica, Bannockburn, IL) with a Cool Snap cf2 camera (Nikon, Melville, NY). Subsequently, the terminal PB was manually circled to quantify the region's mean intensity using NIS Elements BR imaging software (Nikon, Melville, NY). A baseline CY3 intensity value near 0 represents the minimum quantifiable terminal bulb intensity in animals not previously exposed to MitoSOX Red. All MitoSOX analyses were performed by two technicians (S.D. and R.L.); observer influence on mean strain fluorescence intensity was negligible as assessed by ANOVA (see **Section 2.12**).

2.4 Mass spectrometric validation of 2-OH-Mito-E+ production in C. elegans

C. elegans were grown in liquid culture and washed clear of remaining bacteria, as above (**Section 2.1**). Worm number was determined by pelleting washed worms, resuspending them in 50 ml S. basal in Falcon tubes, inverting several times to mix, and counting worm number in triplicate 20 *u*l aliquots under 5X magnification. Approximately 10,000 young adult stage nematodes were fed 10 *u*M MitoSOX in liquid culture in 20°C incubators (I26/R Series, New Brunswick Scientific, Edison, NJ) shaking at 220 rpm for 24 hours, washed three times in 5 ml S. basal, centrifuged at 300g for 5 minutes at 4°C to pellet the worms, and stored at −80°C until use. Three 500 *u*l worm pellets were combined, freeze-thawed twice, and then ground in a homogenizer with a Teflon pestle for 2 minutes on ice. Following the addition of 2 volumes of 100% ethanol, the mixture was further homogenized until approximately 90% of the worms were broken open and the cellular material was freed from the cuticle. Homogenates were incubated on ice in the dark for 1 hour with agitation every 15 minutes, and then centrifuged at 20,000 × G at 4°C for 20 minutes.

Mass spectrometric analysis was performed on worm extract supernatants using an Agilent 1100 series LC-MS instrument equipped with an electrospray (ESI) source and quadrupole mass filter. Synthesis of 2-OH-Mito-E^+ standard was performed as previously described (Zielonka et al. 2008). LC-MS analysis of MitoSOX Red (Mito-HE) and its oxidation products from whole worm extracts was performed as previously published (Zielonka et al. 2008), with slight modification. Reverse phase chromatography was conducted using a Phenomenex Synergi Polar RP column (250mm × 2.0 mm, 4 *u*M), which was directly

coupled to an ESI source operating in positive ion mode. Buffers A and B were 0.1 % formic acid/0.01% trifluoroacetic acid in water and 0.1% formic acid/0.01% trifluoroacetic acid in acetonitrile, respectively. Samples were subjected to a linear gradient at a flow rate of 0.1 ml per min for 35 min from 50 – 75% B. Mito-HE and 2-OH-Mito-E^+ standards (10 pmol) were used to optimize LC-MS single ion monitoring parameters. Initially, full scan spectra (m/z = 200 – 800) were repeatedly acquired over the linear gradient to determine retention time, charge state(s), and m/z value(s). The following m/z values were used during SIM analyses: Mito-HE (Group 1): 632.2 and 316.6 for the singly and doubly-charged molecular ions, respectively; 2-OH-Mito-E^+ (Group 2): 323.6 (2+) for the doubly-charged molecular ion. Aliquots of ethanol extracts (40 *u*l) were analyzed by LC-SIM-MS with a cycle time of 1.20 sec and peak width of 0.2.

2.5 Quantitation of mitochondria membrane potential and mitochondria density by fluorescence microscopy

Young adult worms were incubated for 24 hours at 20°C on NGM plates spread with OP50 *E. coli* that were pre-treated for relative quantitation of mitochondria membrane potential with 1 *u*M tetramethylrhodamine ethyl ester perchlorate (TMRE) and of mitochondria density with 10 *u*M MitoTracker Green FM (Invitrogen, Carlsbad, CA) (Scaduto and Grotyohann 1999). Worms were subsequently transferred to fresh NGM plates containing only OP50 *E. coli* for one hour to clear their intestinal tract of residual dye, after which they were paralyzed *in situ* on NGM plates by adding 10 mg/ml levamisole (Sigma, St. Louis, MO). Photographs were immediately taken (MZFLIII, Leica, Bannockburn, IL). Terminal PB mean fluorescence was quantified using NIS Elements Imaging software (Nikon, Melville, NY), as described above, except that an exposure time of 320 milliseconds and CY3 filter were used. All TMRE analyses were performed by a single technician (S.D.).

2.6 Confocal microscopy

Confocal microscopy (TCS SP2, Leica, Bannockburn, IL) was used to confirm subcellular fluorescence localization within the terminal PB of wild-type and mutant worms (with the assistance of Andrea Stout, Ph. D in the Cell Biology Core Facility, University of Pennsylvania, Philadelphia, PA). Worms were exposed for 24 hours individually or in combination to a MitoTracker Dye (Green, Red, or Deep Red, Invitrogen, Molecular Probes, Carlsbad, CA), MitoSOX (Mito-HE), or TMRE. Following one hour intestinal clearing on unlabelled *E. coli*, nematodes were paralyzed onto glass slides in 20 *u*l of 10 mg/ml levamisole. Double labeling of was not reproducibly achieved due to extensive dye bleed-through at multiple concentrations attempted. Optical stacks were obtained at 1 *u*m resolution, and recombined into movie files using Image J (http://rsbweb.nih.gov/ij/).

2.7 Mitochondria-fraction isolation from C. elegans

When a majority of animals had reached adult stage following growth for a single generation in liquid culture, worms were washed extensively in S. basal with sucrose gradient centrifugation protocol to separate the adult population, as previously described (Falk et al. 2006). The adult-enriched nematode fraction was immediately subject to a mitochondria isolation protocol on ice involving homogenization, proteinase degradation of the outer nematode cuticle, and differential centrifugation, as previously described (Falk et al. 2006), exception an additional slow centrifugation spin (300 × G, 10 minutes, 4°C) was performed to remove remaining intact worms from the mitochondria fraction prior to the first high-speed centrifugation spin (7000 × G, 10 minutes, 4°C).

2.8 Quantitation of sod-2 and sod-3 RNA expression in nematodes at baseline and following paraquat exposure

Worms of each strain were grown to high density on two 10 cm NGM agar plates seeded with OP50 *E. coli*. Synchronous first-day young adult worms of each strain were incubated at 20°C for 24 hours on 10 cm NGM plates with and without 1 mM paraquat. Total RNA was extracted from populations of 1,000 nematodes (estimated by dilution, as per **Section 2.4**) using modified Trizol protocol (Invitrogen Corporation, Carlsbad, CA) and purified in RNeasy spin columns (Qiagen, Inc., Valencia, Ca), as previously described (Falk et al. 2008). Total RNA concentration and dissolution was determined spectrophotometrically at 230 nm, 260 nm, and 280 nm wavelengths (Nanodrop ND-100 Spectrophotometer v3.1.2, NanoDrop Technologies, Inc., Wilmington, DE). 2–10 *u*g of total RNA was DNase-treated using the TURBO DNA-free kit (Ambion Inc., Austin, TX). 400 ng–1.4 *u*g of DNase-treated RNA was reverse transcribed in a 20μl reaction mixture to generate cDNA using High Capacity cDNA Reverse Transcription Kit (Applied Biosystems, Foster City, CA). 40 ng of cDNA was used per quantitative PCR (qPCR) reaction containing Taqman gene expression assays (Applied Biosystems, Foster City, CA) for endogenous housekeeping gene *drs-1* (Ce02451127_g1), as well as the target genes *sod-2* (Ce02410777_g1) or *sod-3* (Ce02404515_g1). *drs-1* was selected based on analysis of genes having unchanging expression in *C. elegans* mitochondria mutants relative to N2 in previously reported expression microarray datasets (Falk et al. 2008) that are publicly accessible (GEO series accession number GSE9967) at NCBI Gene Expression Omnibus (http://www.ncbi.nlm.nih.gov/geo/). Taqman Universal PCR Master Mix (Applied Biosystems, manufactured by Roche, Branchburg, NJ) was used per Applied Biosystems standard protocol for Taqman Gene Expression Assay (Taqman MGB Probes, FAM dye-labeled). Real-time qPCR was performed on a SDS-7500 qPCR machine (Applied Biosystems, Foster City, CA) that was available in the Nucleic Acid and Protein Core Facility at The Children's Hospital of Philadelphia (Philadelphia, PA). Sequence Detection Software 1.2.3 version was used to perform relative quantitation analysis of gene expression (Applied Biosystems, Foster City, CA). Nematode growth and RNA extraction was performed by the same technician (M.R). All qPCR studies were performed by a single individual (E.P.).

2.9 MnSOD enzyme activity assay in C. elegans isolated mitochondria

Mitochondria MnSOD-specific activity was measured by slight modification of the assay described by McCord and Fridovich (McCord and Fridovich 1969). Intact mitochondria were isolated from *C. elegans* (**Section 2.7**), and frozen in −80°C until subsequently being thawed on ice for MnSOD activity analysis. The assay buffer contained 50 mM KH_2PO_4 (Fisher Scientific, Pittsburgh, PA) pH 7.8, 200 *u*M xanthine (Sigma, St. Louis, MO), 60 *u*M acetylated-cytochrome-C (Sigma) 0.02 % Triton-X100 (Sigma), 2 mM KCN (to inhibit any contaminating Cu/Zn SOD) and 0.02 U xanthine oxidase (Calbiochem, San Diego, CA). The rate of acetylated-cytochrome C reduction was measured spectrophotometrically at 550 nm using an Olis Modernized DW-2/2000 Spectrophotometer and Olis Global Works software (Mitochondria Research Core Facility, The Children's Hospital of Philadelphia, Philadelphia, PA). In a single cuvette reaction, a baseline reduction rate was first observed without mitochondria present. Mitochondria protein was then added to the cuvette and the change in the rate of acetylated-cytochrome C reduction was recorded. The rate of reduction in the presence and absence of mitochondria sample was determined using Olis Global Works software. The amount of MnSOD presence in each mitochondria sample was calculated with the following formula (adapted from Kuthan et al. 1986): [SOD] (Unit) = $[(V_0/V_1)-1]$/mg protein, where V_0 = the rate of reduction of acetylated-cytochrome C in the absence of protein, and V_1= the rate of reduction of acetylated-cytochrome C in the presence of mitochondria protein. One unit of SOD was defined as the amount required to cause a 50% inhibition in the rate of reduction of acetylated-cytochrome C. As the reaction constant

was not linear, values were only accepted for mitochondria samples that fell within a 40% to 60% rate reduction. Mean ± SEM MnSOD enzyme activity was determined by averaging a minimum of two technical replicates for each of at least two independent mitochondria preparations of each strain. All analyses were performed by a single individual (E.P.).

2.10 MnSOD protein quantitation by Western analysis of C. elegans isolated mitochondria

Mitochondria proteins were prepared and subjected to Western Blot analysis of MnSOD protein levels. Isolated mitochondria proteins that were prepared from different worm strains (as above, per **Section 2.7**), were first diluted to an appropriate concentration with MSM buffer pH 7.0 containing 220 mM mannitol, 70 mM sucrose, and 5 mM MOPS (SIGMA-Aldrich, St. Louis, MO). These samples were then further diluted with Laemmli sample buffer (BIO-RAD Laboratories, Hercules, CA) containing β-mercaptoethanol, in a 1:1 ratio and boiled at 98°C to 100°C for 4 minutes. Equal amounts of protein samples (50 *u*g) were separated on 12% SDS-PAGE (BIO-RAD Mini Protean 3 Cell, BIO-RAD Laboratories, Hercules, CA). Resolved proteins were transferred to nitrocellulose or PVDF membranes using Mini Trans-Blot Cell system (BIO-RAD) and labeled with rabbit polyclonal anti-SOD2 antibody (Abcam Inc., Cambridge, MA) in 1:1000 dilutions. This antibody was designed to detect amino acids 25–222 of human SOD2. Proteins were detected with Infrared IRDYE 680 conjugated goat anti-rabbit IgG in 1:20000 dilution and protein bands were visualized by scanning the membranes with Odyssey Infrared Imaging Systems (LI-COR Biosciences, Lincoln, NE). Intensity of the 22 kDa band in each sample was quantified to determine the relative amount of MnSOD protein in each mutant strain.

2.11 Analysis of 4-HNE protein adducts from isolated mitochondria

Frozen mitochondria protein was thawed on ice and subjected to Western blot analysis of 4-hydroxy-2-nonenal (4-HNE) protein adducts (Catala 2009), following similar preparation as described above (**Section 2.10**). Equal amounts of mitochondria protein (20 *u*g) were separated on 12% SDS-PAGE and transferred to nitrocellulose or PVDF membranes. Resolved proteins were labeled with rabbit anti-HNE (4-hydroxy-2-nonenal) antibody (Alpha Diagnostic International, San Antonio, TX) in 1:1000 dilutions. Proteins were detected with Infrared IRDYE 680 conjugated goat anti-rabbit IgG in 1:20000 dilution and protein bands were visualized by scanning the membranes with Odyssey Infrared Imaging Systems (LI-COR Biosciences, Lincoln, NE).

2.12 Statistical analyses

Two-sided, non-parametric ANOVA analyses were performed in SAS version 9.1 (SAS Institute Inc, Cary, NC) to compare mean intensity differences between strains both when compared to wild-type, and when compared between baseline and following oxidant stress for a given strain for all live worm fluorescence studies (Figures 2 and 3A). Statistical analysis was performed by student's t-test in Excel (Microsoft) for other analyses as indicated, where * $p<0.05$, ** $p<0.01$, and *** $p<0.001$.

3. RESULTS and DISCUSSION

3.1 Ingested MitoSOX dye predominantly localized to mitochondria-rich pharyngeal bulbs in C. elegans

Upon feeding cationic, mitochondria-targeted, fluorescent dyes to *C. elegans*, a consistent pattern of preferential labeling was observed within their mitochondria-dense PB (Figure 1). This mitochondria distribution closely approximates that observed in a previous report of an EGFP-fusion product of the promoter for the mitochondria complex I K09A9.5 (NDUFS2 homologue) subunit (Kayser et al. 2001), which we also observed upon confocal analysis of

that same strain (data not shown; *pKEK* strain obtained from Philip Morgan, M.D. and Margaret Sedensky, M.D., University of Washington, Seattle, WA). Confocal microscopy demonstrated that MitoSOX-based fluorescence assessed 24 hours following dye ingestion localized to PB cytoplasmic organelles measuring approximately one micron in diameter (Figure 1I). MitoSOX fluorescence exhibited similar PB labeling patterns to other mitochondria-localizing dyes (eg. MitoTracker Green). In addition, large fluorescent foci were consistently observed cephalad to the grinder of the terminal PB in multiple strains following MitoSOX treatment, but not after MitoTracker treatment. Confocal microscopy reconstruction (Supplementary Figure 1) demonstrated that these fluorescent foci can be resolved to multiple mitochondrion-sized particles organized into a c-shaped, tripartite structure that appears bilaterally symmetric with two cephalad arms cradling the terminal PB. This fluorescent mitochondria cluster observed with MitoSOX treatment represents an apparently unique structure that is not characteristic of known pharyngeal, neuronal, or support cells (www.wormatlas.org and personal communication with Leon Avery, PhD) (Albertson and Thomson 1976). While the size of the component vesicles that comprise the c-shaped structure are individually consistent with mitochondria, our inability to co-label them with MitoTracker dyes leaves open several possibilities. Possible explanations include that these particular vesicles may represent viable mitochondria that simply fail to co-label due to co-operative loading of the two dyes, depolarized mitochondria in the process of being degraded, or lipophilic structures of non-mitochondria origin.

Optimal nematode exposure times to mitochondria-targeted dyes sufficient to achieve reproducible, steady-state levels of fluorescence within their terminal PB were determined by an initial feeding time-course experiment (Supplementary Figure 2A). In wild-type (N2 Bristol) synchronous young adult nematodes fed 10 *u*M MitoSOX, increased fluorescence was observed between 12 and 36 hours of dye ingestion, whereas exposure times under four hours proved inadequate to permit reproducible fluorescence quantitation. Repeat time-course analyses applying the same experimental conditions and analyses subsequently used in strain comparisons (**Section 3.2**) confirmed that within a single strain, N2 Bristol, 24 hour dye exposure produced highly reproducible results, with fluorescence intensity largely unchanged between 24 and 97 hours of dye exposure (Supplementary Figure 2B). 24 hour dye exposure time to synchronized nematode populations beginning on their first day of adulthood (defined by the first day of egg-laying) was selected for comparative studies between strains (**Section 3.2**), although variable rate of dye uptake between strains may be a potential confounding factor. Live bacteria were used for all experiments, since wild-type nematodes fed dye for prolonged periods (eg. 60 hours) on UV-killed bacteria had poor growth and early death that closely followed observed spikes in relative oxidant levels assessed by mean terminal PB MitoSOX fluorescence, most evident following high-dose (20 mM) paraquat treatment (Supplementary Figure 2A).

Under these feeding conditions, MitoSOX ingestion and subsequent oxidation by superoxide generates a specific product, 2-OH-Mito-E^+, whose production within mitochondria can be detected by LC-MS in worm extracts from the complex I mutant, *gas-1*(*fc21*) (Supplementary Figure 3). MitoSOX can also be oxidized by other oxidants, albeit at lower yields, forming the non-superoxide oxidant product, Mito-E^+, which can also be monitored by LC-MS. A major challenge to *in vivo* detection of superoxide has been the specificity of its detection (Zielonka et al. 2008). As monitoring of the 2-OH-Mito-E^+ product offers a unique opportunity to perform comparative quantitative assessment of superoxide production, the LC-MS data provided here is one of the few examples in the existing literature that support *in vivo* production of superoxide. However, technical limitations of this method prohibited reliable relative quantification of 2-OH-Mito-E^+ production between strains. Therefore, fluorescence microscopy was employed for relative quantification of *in vivo* oxidant levels following MitoSOX exposure in *C. elegans* (**Section 3.2**).

3.2 In vivo matrix oxidant burden was greatest in mutants for RC complex I and MnSOD

In comparison with wild-type (N2), significantly increased baseline MitoSOX fluorescence was observed in *gas-1* (29%, p<0.001), *sod-2(gk257)* (21%, p<0.01), and *sod-3* (29%, p<0.001) mutants (Figure 2, blue bars). The long-lived *daf-2* mutant showed no significant difference in PB fluorescence from N2 (4% decrease, p=0.355). Upon 1 mM paraquat exposure, increased oxidant levels assessed by terminal PB MitoSOX fluorescence relative to N2 were observed in *gas-1* (55%, p<0.001), *mev-1* (21%, p<0.001), *isp-1* (8%, p<0.01), and *sod-3* (17%, p<0.001) (Figure 2, red bars). *In vivo* oxidant burden upon exposure to paraquat remained unchanged in both N2 and the insulin receptor mutant (*daf-2)*, as is consistent with the well-documented oxidative stress resistance of *daf-2* (Feng et al. 2001). Intrastrain comparison of mean terminal PB fluorescence following 1 mM paraquat exposure relative to the same mutant at baseline demonstrated significantly *increased* oxidant levels upon oxidant stress in all three RC mutants: *gas-1* (59%, p<0.01), *mev-1* (21%, p<0.001), and *isp-1* (10%, p<0.001). Surprisingly, intrastrain comparison of two MnSOD mutants, *sod-2*(*gk257*) and *sod-3*(*gk235*), each showed *decreased* oxidant levels by 14% (p<0.001) following 1 mM paraquat treatment. This unanticipated decrease in fluorescence appeared to result from diminished dye uptake due to poor feeding and general activity in the MnSOD mutants, which implies the MnSOD mutants manifest excessive oxidative stress sensitivity rather than resistance. Indeed, all MnSOD mutants appeared sickly and died prematurely following paraquat exposure (data not shown), whereas mortality did not appear to be substantially increased following 24 hour paraquat exposure in the other strains.

3.3 Complex I mutant had most substantially decreased in vivo mitochondria membrane potential

In vivo $\Delta\Psi_m$ measured by TMRE fluorescence was significantly decreased (p<0.001) in all mitochondria mutant strains relative to N2, as is consistent with a recent report using a different fluorescent indicator dye (Lemire et al. 2009). The most dramatic differences were observed in strains harboring mutations in RC complexes that generate the proton gradient (mean fluorescence intensity decreased by 62.7% in *gas-1(fc21)* and by 24.2% in *isp-1*(*qm150*), respectively) as well as in all three MnSOD knockout alleles studied (decreased mean fluorescence by 20% in *sod-2*(*gk257*), 26% in *sod-2*(*ok1030*), and 17% in *sod-3*(*gk235*)) (Figure 3A). As *gas-1* had a substantially less polarized $\Delta\Psi_m$ than did N2 at baseline, increased oxidant levels assessed by MitoSOX fluorescence in this strain are not attributable to changes in mitochondria polarization. Furthermore, study of a reporter dye whose uptake into mitochondria is largely independent of membrane potential (MitoTracker Green FM) showed that *gas-1* had a 48% decrease in mean PB fluorescence intensity, suggesting decreased PB mitochondria density in this complex I mutant (Figure 3B). Thus, the 29% relative increase in MitoSOX PB fluorescence in the complex I mutant was likely an underestimate of mitochondria oxidant burden, since their reduced $\Delta\Psi_m$ and decreased mitochondria content would be predicted to limit MitoSOX uptake and retention.

3.4 Mitochondria superoxide scavenging capacity was most substantially enhanced in complex III dysfunction

C. elegans has two functional MnSOD paralogs (*sod-2* and *sod-3*) that share extensive protein sequence similarity with human *SOD2* (Table 1) (Hunter et al. 1997). Relative quantitation of *sod-2* and *sod-3* expression by qRT-PCR analysis of total RNA isolated from synchronous young adult nematode populations revealed substantially greater transcriptional upregulation of *sod-3* than *sod-2* in all mutants studied (Figure 4A). *sod-2* expression was most upregulated at baseline relative to N2 in *mev-1* (by 2.2-fold), and following paraquat-induced oxidant stress in *gas-1* (by 1.8-fold). By comparison, *sod-3* expression showed dramatically greater upregulation in all RC mutants (*gas-1*, *mev-1*, and *isp-1)* both at

baseline relative to N2 (by 11.5-fold, 8.5-fold, and 15-fold, respectively) (Table 2A) and following oxidative stress relative to paraquat-treated N2 (7.5-fold, 5.5-fold, and 9-fold, respectively) (Table 2B). Intrastrain comparison upon paraquat challenge revealed *sod-2* expression was most increased above baseline levels in *gas-1* (25%), whereas *sod-3* was substantially induced following oxidant stress in all three RC mutants and N2. These data suggest that *sod-3* is the predominant MnSOD gene in *C. elegans* responding to mitochondria oxidative stress caused by primary RC dysfunction. However, determination of absolute *sod-2* vs *sod-3* transcript levels would be necessary to prove the functional significance of this upregulated response.

To assess mitochondria superoxide removal capacity of each mutant strain regardless of individual transcript levels, total MnSOD protein levels (Figures 4B) and MnSOD enzymatic activity (Figure 5) were quantified in intact mitochondria isolated from each strain. MnSOD protein levels were variably increased in the RC mutants (73% in *gas-1*, 10-fold in *mev-1*, and 8-fold in *isp-1*) (Table 2B). However, MnSOD enzyme activity was only significantly increased in the complex III mutant, *isp-1* (by 2-fold) relative to N2. MnSOD enzyme activity showed non-significant trends toward increase in *gas-1*, *daf-2*, and *sod-3(gk235),* and was essentially unchanged in *mev-1*. Thus, increased MnSOD transcript did not translate to similar magnitude increases in MnSOD protein or enzyme activity in all strains. We postulate that MnSOD is itself a target of oxidant damage in *C. elegans*.

3.5 Altered longevity in mitochondria RC mutants correlated directly with oxidant scavenging capacity and indirectly with in vivo oxidant levels

High-throughput assessment of mutant lifespan in the presence of FUDR validated previous reports of decreased longevity in complex I RC mutants (Kayser et al. 2004), and increased longevity in complex III RC mutants (Feng et al. 2001) and insulin receptor mutants (Kenyon et al. 1993) (Supplementary Figure 4). In contrast to prior reports of shortened lifespan in *mev-2*(*kn1*) (Honda 2008), FUDR-based lifespan analysis of the complex II mutant was unaltered relative to N2. A modest increase in median lifespan was observed for the MnSOD mutants relative to N2, although this was largely limited to *sod-2* (9% and 4% increased median lifespan in the *ok1030* and *gk257* knockout alleles, respectively) rather than *sod-3* (0.5% increased median lifespan in the *gk257* knockout allele). While these data were consistent with increased longevity recently reported in *sod-2* (Van Raamsdonk and Hekimi 2009), we observed a less dramatic effect. Furthermore, the magnitude of altered longevity of any MnSOD mutant allele did not approximate that seen for the complex III RC mutant (43% increased median lifespan in *isp-1*(*qm150*)).

We observed that MnSOD induction is common to many RC mutants and does not alone predict lifespan. However, correlation of longevity with *in vivo* matrix oxidant burden in RC mutants demonstrated substantially increased *in vivo* oxidant levels and reduced oxidant scavenging capacity in the short-lived complex I mutant (*gas-1*(*fc21*)) relative to the long-lived complex III mutant (*isp-1*(*qm150*)) (Table 2). These data suggest that greater MnSOD enzyme scavenging capacity is associated with lower *in vivo* oxidant levels and increased longevity in the setting of primary RC dysfunction. Study of additional RC complexes and mutations will be necessary to determine the generalizability of this association in primary RC dysfunction.

Oxidant damage assessed by immunoreactive 4-HNE protein adducts in isolated mitochondria was modestly increased in all RC mutants (similarly as previously reported in *gas-1*(*fc21*) and *mev-1*(*kn1*) by Kayser et al. 2004) and MnSOD mutants, but not in the insulin receptor mutant (Supplementary Figure 5). The extent of 4-HNE adducts did not correlate with animal longevity (Table 2). Indeed, the complex II mutant having the least

change in lifespan had the greatest increase in 4-HNE adducts (50% increase in *mev-1* relative to N2).

3.6 Biological relevance

Understanding the complex relationship between oxidant stress and altered longevity in genetically-based mitochondrial RC dysfunction is facilitated by integrated analysis of the *in vivo* effects of individual mutations on oxidant levels, membrane potential, and lifespan, along with *in vitro* assessment of mitochondria superoxide scavenging capacity and lipid peroxidation damage in *C. elegans.* Application of novel methods to quantify mitochondria-specific fluorescence in living animals permits sensitive assessment of relative mitochondria membrane potential and matrix oxidant levels, both in individual genetic mutations and/or with oxidative stress. While MitoSOX PB fluorescence quantitation permits assessment of matrix oxidant burden, oxidant production from enzymes that release oxidants into the intermembrane space will not be measured by this approach. Quantifying terminal PB fluorescence is preferable to whole-worm fluorescence quantification for enhancing the sensitivity and specificity of functional mitochondria assessment owing to the high mitochondria density in the PB, while minimizing effects attributable to the lipophilic quality of the dyes that enables their binding to non-mitochondria organelles, such as lipid-rich gut granules. However, this approach necessitates manual analysis of a large number of individual animals to discern whether relative differences in mitochondrial function are attributable to a specific mutation, exposure, or stochastic variation. Development of computer algorithms to specifically quantify terminal PB fluorescence is a future goal to enhance the practical utility of this approach. A potential alternative approach to permit quantitation of whole animal fluorescence is to assess mitochondria-localized dyes in animals lacking lipophilic gut granules (such as the lysosomal mutant, *glo-1*) (Hermann et al. 2005). However, we did not pursue this approach to avoid potentially confounding effects of combined lysosomal and mitochondrial dysfunction.

The only mutants in our study that had significantly increased *in vivo* oxidant levels were the complex I mutant (*gas-1*) and two paralogous MnSOD mutants, *sod-2(gk257)* and *sod-3(gk235)* (Figure 2). Since complex I is the major site for matrix oxidant production (Hirst et al. 2008), it is reasonable to postulate that the *gas-1* (*NDUFS2*) mutation would increase oxidant production due to its location in the complex I matrix arm along the pathway of electron transfer and near the presumed site of oxidant production. With oxidant stress caused by prolonged paraquat exposure, however, all three RC mutants showed increased *in vivo* matrix oxidant levels despite concordant robust MnSOD induction. Although absolute transcript quantitation was not performed, relative quantitation suggested *sod-3* induction far exceeded that of *sod-2* in all RC mutants. Regardless, greater than 11-fold upregulation of *sod-3* in the complex I mutant, *gas-1*(*fc21*) proved inadequate to compensate for ongoing increased oxidant production by inherently mutant mitochondria. Similarly, 2-fold increased *sod-3* transcript levels in *sod-2*(*gk257*) knockouts were insufficient to scavenge that mutant's *in vivo* oxidant load despite its having presumably normal inherent mitochondrial RC composition. Both mutant MnSOD paralogs studied displayed significantly increased *in vivo* matrix oxidant levels, which was greater in *sod-3*(*gk235*) relative to *sod-2*(*gk257*). Interestingly, although lifespan of both of these MnSOD paralog knockouts were perhaps marginally increased relative to wild-type, we and others observed the extent to be less pronounced than for *sod-2* (*ok1030*) (Van Raamsdonk and Hekimi 2009). The *sod-2* knockout allele initially assessed by *in vivo* fluorescence studies of matrix oxidant burden was *sod-2*(*gk257*), although subsequent inclusion of the *sod-2*(*ok1030*) allele did not demonstrate substantial differences between the two *sod-2* mutants in analyses of *in vivo* membrane potential or mitochondria MnSOD enzyme activity. Overall, both MnSOD paralogous genes clearly contribute to mitochondria oxidant

scavenging capacity in *C. elegans*, as knockout of either increases *in vivo* oxidant levels and loss of *sod-2* alone reduces *in vitro* superoxide scavenging activity. However, *sod-3* appears to be the primary MnSOD transcript induced by primary RC dysfunction.

As fluorescence-based oxidant quantitation requires mitochondria uptake of positively charged dyes, we investigated whether impaired membrane potential and/or altered mitochondria density accounted for MitoSOX fluorescence differences in the RC mutants. We observed that *in vivo* membrane potential was significantly decreased in all RC mutants relative to wild-type, and most substantially reduced in the complex I mutant where mean TMRE fluorescence intensity was decreased by 63% in *gas-1(fc21)* (Figure 3A). Therefore, the observed 29% increase in MitoSOX fluorescence in the complex I mutant cannot be attributed to altered membrane potential, but likely represents an underestimate of the actual *in vivo* oxidant levels occurring consequent to complex I dysfunction. When also factoring in the nearly 50% decrease in MitoTracker Green FM fluorescence quantitation seen in *gas-1* relative to N2 suggestive of decreased mitochondria density (Figure 3B), corrected MitoSOX fluorescence quantitation would exceed a 2-fold increase in the complex I mutant, although TMRE and MitoTracker dye uptake might not truly be independent. Similarly, relatively increased MitoSOX fluorescence levels identified in the other RC mutants also likely provide underestimations of their *in vivo* oxidant burden to an extent that is proportionate to their relative reduction in mitochondria membrane potential. In other words, a *linear* reduction in mitochondria membrane potential will result in an *exponential* reduction in the amount of MitoSOX loaded into the mitochondria and hence available for oxidation. Nonetheless, relative analysis of oxidant levels and mitochondria membrane potential in three primary RC mutants using fluorescence microscopy suggests that complex I function may make the largest contribution to *in vivo* membrane potential. An alternative possibility may be that observed fluorescence alterations are attributable to the specific RC subunit and amino acid residue affected in each of the three RC mutants studied, rather than generalizable to the normal function of their respective complexes. Since membrane potential follows a logarithmic scale, it is also possible that the millivolt differences in membrane potential in living nematodes are not as great between the RC mutants studied as would be suggested by linear-scale fluorescence analyses.

Correlation of longevity with *in vivo* oxidant assessment in mitochondrial RC mutants demonstrated substantially greater oxidant stress based on increased matrix oxidant levels as well as reduced mitochondria oxidant scavenging *capacity* in the short-lived, complex I mutant (*gas-1*(*fc21*)) relative to the long-lived, complex III mutant (*isp-1*(*qm150*)). In contrast, upregulated MnSOD *expression* was common to all three RC mutants and did not predict lifespan, perhaps because of oxidant-induced impairment of MnSOD activity in some cases. These data suggest that greater MnSOD enzyme scavenging capacity is associated with lower *in vivo* oxidant levels and increased longevity in the setting of primary RC dysfunction. Study of additional RC complexes and mutations will be necessary to determine the generalizability of this association in primary RC dysfunction.

Our data further demonstrate that *daf-2* mutants have a less robust increase in MnSOD expression and enzyme activity than do the complex III mutants. However, matrix scavenging capacity proved sufficient in *daf-2* but insufficient in *isp-1* to prevent increased *in vivo* matrix oxidant burden following oxidant stress. Furthermore, a greater than two-fold increased median lifespan in the insulin receptor mutant (*daf-2*(*e1368*)) relative to any RC mutant further supports that the mechanism of longevity due to altered insulin/FOXO signaling pathway is distinct from that caused by primary RC dysfunction and not solely attributable to oxidative stress, as is consistent with prior studies (Honda and Honda 1999).

4. CONCLUSION

C. elegans is a microscopically transparent, multi-cellular animal whose muscle tube-like, continually pumping pharynx is densely populated by mitochondria that can be readily and preferentially labeled with targeted fluorescent dyes. *C. elegans* terminal PB fluorescence quantitation thus offers a sensitive and specific means of non-invasively monitoring relative, steady-state, *in vivo* mitochondria oxidant burden and membrane potential. Targeted analyses of the seven-cell, terminal PB tissue in living *C. elegans* mutants for three different RC complexes, two MnSOD paralogous genes, and the insulin receptor demonstrated that significantly *increased* MitoSOX fluorescence and *reduced* TMRE fluorescence, indicative of increased matrix oxidant burden and decreased $\Delta\Psi_m$, respectively, occur only in mutants for RC complex I, *gas-1*(*fc21*), and two *C. elegans* paralogs of human *SOD2* (MnSOD). Upon exposure to the oxidant generating agent, paraquat, *in vivo* oxidant levels rose most substantially in the short-lived complex I mutant, *gas-1*(*fc21*), and near normal-lived complex II mutant, *mev-1*(*kn1*), despite robust MnSOD induction at the level of expression (primarily *sod-3*) in both and at the protein level in *mev-1*(*kn1*). However, significantly increased MnSOD *enzyme activity* only occurred in the long-lived complex III mutant, *isp-1*(*qm150*), whose *in vivo* oxidant burden was notably not elevated. Thus, greater MnSOD scavenging capacity was associated with lower *in vivo* mitochondria oxidant burden and increased longevity in the setting of primary RC dysfunction, particularly when comparing the complex III (*isp-1*(*qm150*)) and complex I (*gas-1*(*fc21*)) mutations. Nevertheless, *isp-1*(*qm150*) manifested modest oxidative stress sensitivity and only half as prolonged median lifespan as the longer-lived insulin receptor, *daf-2*(*e1368*) mutant. Furthermore, modestly increased longevity was seen in a MnSOD knockout (*sod-2*) that had decreased MnSOD scavenging capacity and increased *in vivo* oxidant burden. Thus, factors beside oxidant stress must underlie RC mutant longevity in *C. elegans*.

Supplementary Material

Refer to Web version on PubMed Central for supplementary material.

Acknowledgments

This work was funded by NIH grant K08-DK073545 and Ellison Medical Foundation New Scholar's Award in Aging (AG-NS-0327-06) (MJF) as well as supported by the Gisela and Dennis Alter Chair in Pediatric Neonatology, and the Joseph Strokes Jr. Investigator program (HI). We thank Alexandra Gladstone for her assistance developing *C. elegans* fluorescence-based membrane potential analyses; Andrea Stout, PhD, of the Cell Biology Confocal Core Facility at The University of Pennsylvania School of Medicine for her expertise in confocal microscopy and movie generation; Todd Lamitina, PhD, for his helpful discussions and guidance in fluorescence microscopy; Evgueni Daikhin, MD, PhD and Marc Yudkoff, MD of the CHOP Mass Spectrometry Core Facility for their assistance with MS validation of MitoSOX specific products; Mary Selak, PhD, for her assistance in optimizing the MnSOD enzyme activity assay; Philip G. Morgan, M.D. and Margaret M. Sedensky, M.D. for sharing the *pKEK* EGFP mutant strain; as well as Abdul Salam, PhD of Westat Statistical Core and Zhe Zhang, PhD of the CHOP Bioinformatics Core for their assistance with statistical analyses and generation of Figures 2 and 3, respectively.

Abbreviations

C. elegans	*Caenorhabditis elegans*
MnSOD	manganese superoxide dismutase
RC	respiratory chain
PB	pharyngeal bulb

References

Albertson DG, Thomson JN. The pharynx of Caenorhabditis elegans. Philos Trans R Soc Lond B Biol Sci. 1976; 275(938):299–325. [PubMed: 8805]

Altun ZF, Hall DH. 2008Alimentary System: Pharynx. WormAtlas. http://www.wormatlas.org/hermaphrodite/pharynx/mainframe.htm

Avery L, Horvitz HR. Pharyngeal pumping continues after laser killing of the pharyngeal nervous system of C. elegans. Neuron. 1989; 3(4):473–85. [PubMed: 2642006]

Balaban RS, Nemoto S, Finkel T. Mitochondria, oxidants, and aging. Cell. 2005; 120(4):483–95. [PubMed: 15734681]

Bus JS, Gibson JE. Paraquat: model for oxidant-initiated toxicity. Environ Health Perspect. 1984; 55:37–46. [PubMed: 6329674]

Catala A. Lipid peroxidation of membrane phospholipids generates hydroxy-alkenals and oxidized phospholipids active in physiological and/or pathological conditions. Chem Phys Lipids. 2009; 157(1):1–11. [PubMed: 18977338]

Chen Q, et al. Production of reactive oxygen species by mitochondria: central role of complex III. J Biol Chem. 2003; 278(38):36027–31. [PubMed: 12840017]

Clokey GV, Jacobson LA. The autofluorescent “lipofuscin granules” in the intestinal cells of Caenorhabditis elegans are secondary lysosomes. Mech Ageing Dev. 1986; 35(1):79–94. [PubMed: 3736133]

Cocheme HM, Murphy MP. Chapter 22 The uptake and interactions of the redox cycler paraquat with mitochondria. Methods Enzymol. 2009; 456:395–417. [PubMed: 19348901]

DiMauro S. Mitochondrial diseases. Biochim Biophys Acta. 2004; 1658(1–2):80–8. [PubMed: 15282178]

Falk MJ, et al. Mitochondrial complex I function modulates volatile anesthetic sensitivity in C. elegans. Curr Biol. 2006; 16(16):1641–5. [PubMed: 16920626]

Falk MJ, et al. Metabolic pathway profiling of mitochondrial respiratory chain mutants in C. elegans. Mol Genet Metab. 2008; 93(4):388–97. [PubMed: 18178500]

Feng J, Bussiere F, Hekimi S. Mitochondrial electron transport is a key determinant of life span in Caenorhabditis elegans. Dev Cell. 2001; 1(5):633–44. [PubMed: 11709184]

Gaskova D, DeCorby A, Lemire BD. DiS-C3(3) monitoring of in vivo mitochondrial membrane potential in C. elegans. Biochem Biophys Res Commun. 2007; 354(3):814–9. [PubMed: 17266929]

Hamilton B, et al. A systematic RNAi screen for longevity genes in C. elegans. Genes Dev. 2005; 19(13):1544–55. [PubMed: 15998808]

Hermann GJ, et al. Genetic analysis of lysosomal trafficking in Caenorhabditis elegans. Mol Biol Cell. 2005; 16(7):3273–88. [PubMed: 15843430]

Hirst J, King MS, Pryde KR. The production of reactive oxygen species by complex I. Biochem Soc Trans. 2008; 36(Pt 5):976–80. [PubMed: 18793173]

Honda Y, Honda S. The daf-2 gene network for longevity regulates oxidative stress resistance and Mn-superoxide dismutase gene expression in Caenorhabditis elegans. FASEB J. 1999; 13(11):1385–93. [PubMed: 10428762]

Honda Y, Tanaka M, Honda S. Modulation of longevity and diapause by redox regulation mechanisms under the insulin-like signaling control in Caenorhabditis elegans. Exp Gerontol. 2008; 43(6):520–529. [PubMed: 18406553]

Hope, IA. C. elegans A practical approach. Oxford, UK: Oxford University Press; 1999.

Hunter T, Bannister WH, Hunter GJ. Cloning, expression, and characterization of two manganese superoxide dismutases from Caenorhabditis elegans. J Biol Chem. 1997; 272(45):28652–9. [PubMed: 9353332]

Kayser EB, et al. Mitochondrial expression and function of GAS-1 in Caenorhabditis elegans. J Biol Chem. 2001; 276(23):20551–8. [PubMed: 11278828]

Kayser EB, Sedensky MM, Morgan PG. The effects of complex I function and oxidative damage on lifespan and anesthetic sensitivity in Caenorhabditis elegans. Mech Ageing Dev. 2004; 125(6): 455–64. [PubMed: 15178135]

Kenyon C, et al. A C. elegans mutant that lives twice as long as wild type. Nature. 1993; 366(6454): 461–4. [PubMed: 8247153]

Kuthan H, Haussmann HJ, Werringloer J. A spectrophotometric assay for superoxide dismutase activities in crude tissue fractions. Biochem J. 1986; 237(1):175–80. [PubMed: 3026308]

Lemire BD, et al. C. elegans longevity pathways converge to decrease mitochondrial membrane potential. Mech Ageing Dev. 2009; 130(7):461–5. [PubMed: 19442682]

McCord JM, Fridovich I. An enymatic function for erythrocuprein (Hemocuprein). J of Bio Chem. 1969; 244:6049–55. [PubMed: 5389100]

Murphy MP. How mitochondria produce reactive oxygen species. Biochem J. 2009; 417(1):1–13. [PubMed: 19061483]

O'Reilly CM, et al. Quantitative analysis of spontaneous mitochondrial depolarizations. Biophys J. 2003; 85(5):3350–7. [PubMed: 14581236]

Rea SL, Ventura N, Johnson TE. Relationship between mitochondrial electron transport chain dysfunction, development, and life extension in Caenorhabditis elegans. PLoS Biol. 2007; 5(10):e259. [PubMed: 17914900]

Robinson KM, Janes MS, Beckman JS. The selective detection of mitochondrial superoxide by live cell imaging. Nat Protoc. 2008; 3(6):941–7. [PubMed: 18536642]

Scaduto RC Jr, Grotyohann LW. Measurement of mitochondrial membrane potential using fluorescent rhodamine derivatives. Biophys J. 1999; 76(1 Pt 1):469–77. [PubMed: 9876159]

Schapira AH. Mitochondrial disease. Lancet. 2006; 368(9529):70–82. [PubMed: 16815381]

Shtonda B, Avery L. CCA-1, EGL-19 and EXP-2 currents shape action potentials in the Caenorhabditis elegans pharynx. J Exp Biol. 2005; 208(Pt 11):2177–90. [PubMed: 15914661]

Starich TA, et al. eat-5 and unc-7 represent a multigene family in Caenorhabditis elegans involved in cell-cell coupling. J Cell Biol. 1996; 134(2):537–48. [PubMed: 8707836]

Valko M, et al. Free radicals, metals and antioxidants in oxidative stress-induced cancer. Chem Biol Interact. 2006; 160(1):1–40. [PubMed: 16430879]

Van Raamsdonk JM, Hekimi S. Deletion of the mitochondrial superoxide dismutase sod-2 extends lifespan in Caenorhabditis elegans. PLoS Genet. 2009; 5(2):e1000361. [PubMed: 19197346]

Yang W, Li J, Hekimi S. A Measurable increase in oxidative damage due to reduction in superoxide detoxification fails to shorten the life span of long-lived mitochondrial mutants of Caenorhabditis elegans. Genetics. 2007; 177(4):2063–74. [PubMed: 18073424]

Zielonka J, Vasquez-Vivar J, Kalyanaraman B. Detection of 2-hydroxyethidium in cellular systems: a unique marker product of superoxide and hydroethidine. Nat Protoc. 2008; 3(1):8–21. [PubMed: 18193017]

Zuryn S, Kuang J, Ebert P. Mitochondrial modulation of phosphine toxicity and resistance in Caenorhabditis elegans. Toxicol Sci. 2008; 102(1):179–86. [PubMed: 17998274]

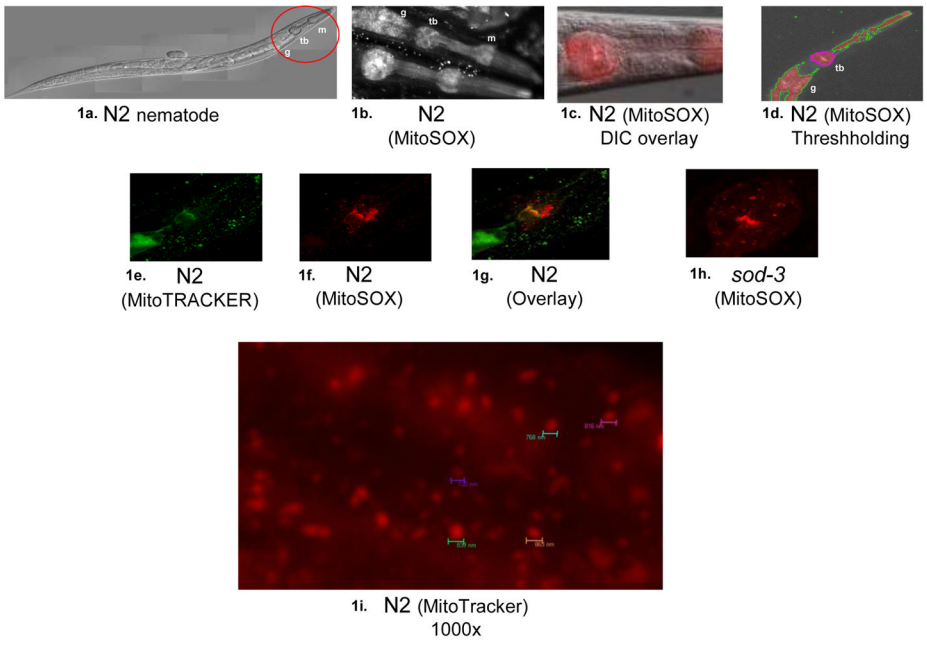

Figure 1. Nematode terminal pharyngeal bulb labeling with mitochondria-targeted dyes

a) Light micrograph of young adult wild-type (N2) nematode, where cephalad portion (red circle) highlights the two pharyngeal bulbs (m, metacorpus and tb, terminal bulb) and initial portion of the gastrointestinal tract (g); **b)** MitoSOX fluorescence in N2 demonstrates consistent labeling within the *C. elegans* pharynx, as well as in lipid-rich gut granules that non-specifically bind lipophilic dyes. The top worm shows nuclear sparing of the mitochondria-localized dye both in the terminal pharyngeal bulb (tb) and in cells of the gastrointestinal tract (g); **c)** MitoSOX fluorescence of N2 pharynx overlay with DIC image demonstrates preferential labeling in terminal pharyngeal bulb; **d)** Threshholding permits focused analysis of terminal pharyngeal bulb (tb) fluorescence. Similar fluorescent patterns were observed by confocal microscopy maximal projection images whether animals are fed: **e)** MitoTracker Green in N2, **f)** MitoTracker Red in N2, **g**) Overlay of e and f, **h)** Typical MitoSOX terminal pharyngeal bulb fluorescent pattern in *sod-3* knockout mutant, **i)** 1000x magnification image taken with CY3 filter of N2 fed MitoTracker Red demonstrated individual cytoplasmic vesicle labeling on the order of ~800 nm diameter fluorescent foci.

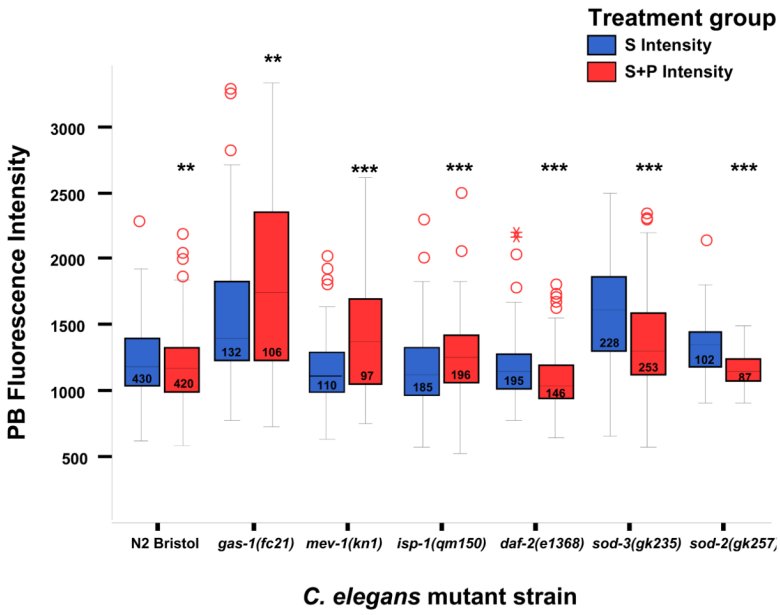

Figure 2. *In vivo* relative oxidant quantitation in *C. elegans* terminal pharyngeal bulbs

Steady-state oxidant levels in young adult nematodes at baseline as determined by mean terminal pharyngeal bulb (PB) fluorescence at 160X magnification at baseline and following 24 hour exposure to 10 *u*M MitoSOX Red ("S" = baseline, blue bars) ± 1 mM paraquat ("S +P" = oxidant stress, red bars) at 20°C. Steady-state oxidant levels were significantly *increased* only in the complex I and both MnSOD paralog knockout mutants. With paraquat exposure, *in vivo* relative oxidant levels rose significantly in all three RC mutants (*gas-1, mev-1, isp-1*). Statistical analyses were performed by ANOVA, where ** $p<0.01$, *** $p<0.001$). Box length represents 25th to 75th percentile inter-quartile range, interior horizontal line represents median, vertical lines issuing from the box extend to minimum and maximum values of the adjacent analysis variable [calculated as third quartile ± (1.5*interquartile range)], open red circles indicate outliers defined as values exceeding the upper adjacent level, and asterisks represent severe outliers (exceed 3 box lengths above the upper adjacent level). N, total animal number studied over three replicate experiments per strain, as indicated within boxes. *sod-2* strain presented is *sod-2*(*gk235*).

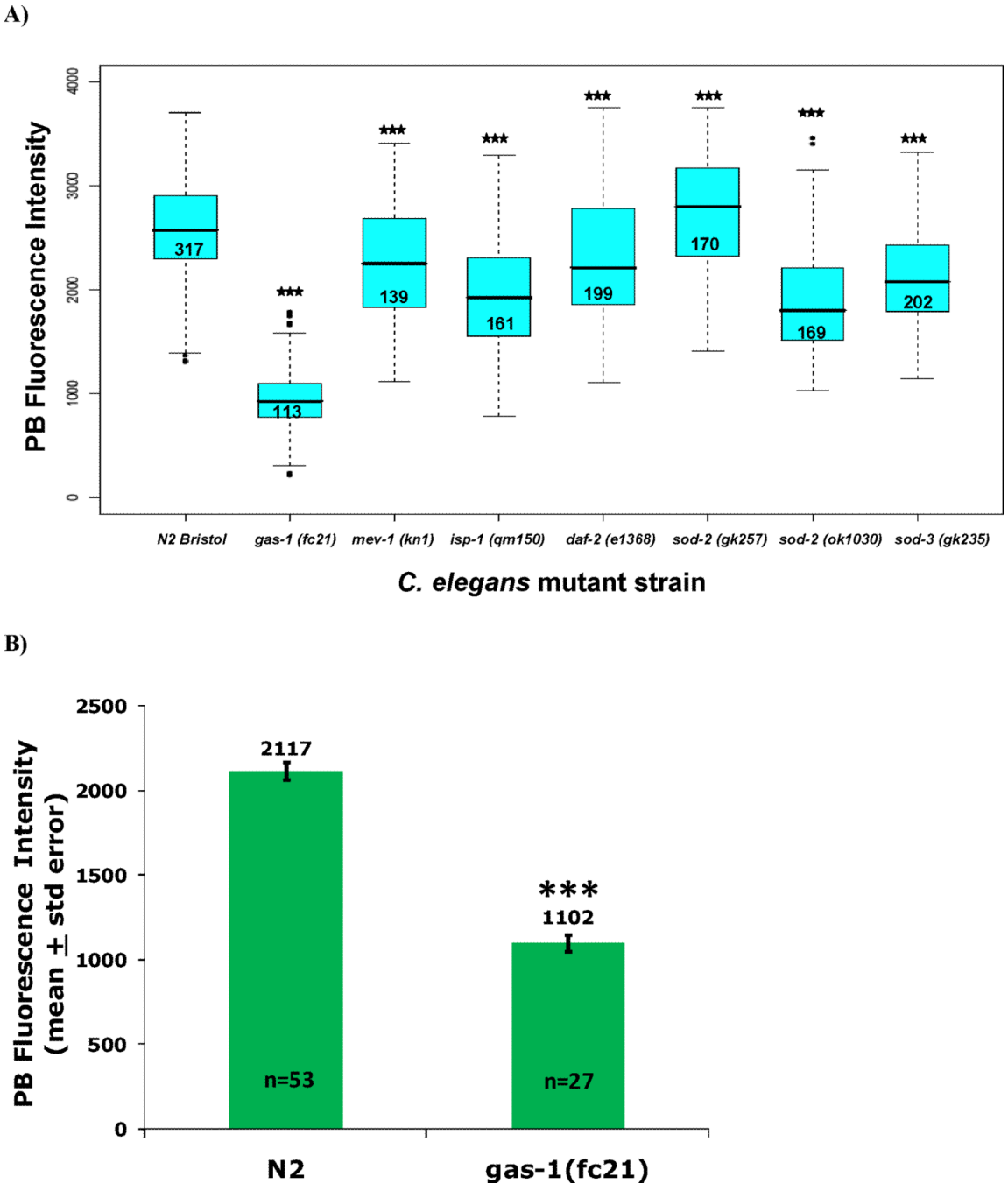

Figure 3. ***In vivo*** **quantitation of relative membrane potential and mitochondria density in** ***C. elegans*** **terminal pharyngeal bulbs**

A) Mitochondria membrane potential ($\Delta\Psi_m$) in living nematodes at baseline as determined by mean fluorescence at 160X magnification following 24 hour exposure to 1 *u*M TMRE at 20°C. $\Delta\Psi_m$ was most dramatically reduced relative to wild-type (N2) in the complex I mutant (*gas-1*, mean PB fluorescence decreased by 63%). Mean TMRE PB fluorescence was also substantially reduced in the complex III mutant (*isp-1*) and both *sod-2* mutants, but was only decreased by 12% in the complex II mutant (*mev-1*) and by 9% in the insulin receptor mutant (*daf-2*). Statistical analyses were performed by ANOVA, where *** p<0.001). Box plot components indicate values as detailed in Figure 2 legend. N, total

animal numbers studied across three replicate experiments per strain, as indicated within boxes. B) Decreased mitochondria density in complex I mutant worms is suggested by a 48% decrease in mean PB fluorescence intensity in *gas-1* relative to N2 following 24 hour exposure of synchronous young adult worms to 10 *u*M MitoTracker Green FM dye, whose mitochondria localization is largely independent of membrane potential. Statistical analysis by student's t-test, where *** $p<0.001$. N, animal number studied per strain. PB, pharyngeal bulb.

a)

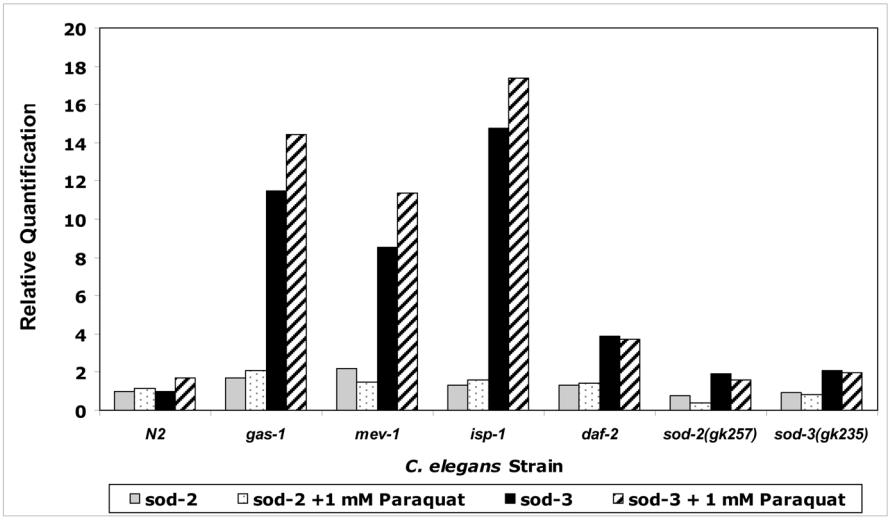

b)

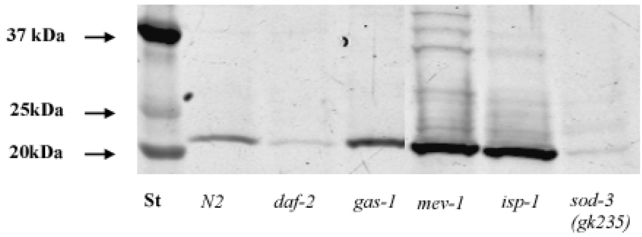

c)

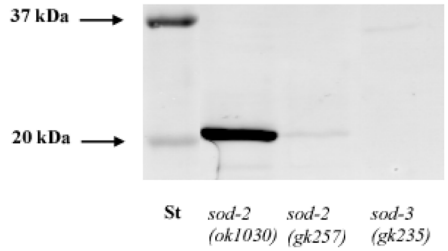

Figure 4. Whole worm MnSOD expression and protein levels in mitochondria mutants

A) Whole worm MnSOD total RNA levels were measured by qPCR. *sod-3* upregulation dramatically exceeded *sod-2* upregulation in primary RC dysfunction, both at baseline and following oxidant stress. **B)** MnSOD western blot analysis in isolated mitochondria from RC mutant strains confirmed that total MnSOD protein is upregulated (22kDa band) in RC mutants (complex I, *gas-1*; complex II, *mev-1*, and complex III, *isp-1*). By contrast, MnSOD protein was not increased in the insulin receptor mutant (*daf-2*), despite its 4-fold increased *sod-2* transcript level (**Figure 4A, above**). MnSOD protein levels were diminished relative to N2 in the *sod-3* MnSOD knockout mutant, suggesting both *sod-2* and *sod-3* contribute to

total MnSOD protein levels. **C)** MnSOD western blot analysis in isolated mitochondria from three distinct knockout alleles of two *sod-2* paralogs again demonstrated decreased MnSOD in an independent mitochondria preparation of *sod-3*(*gk235*), mutant as well as decreased MnSOD in the *sod-2*(*gk257*) compound heterozygous deletion/insertion allele. However, MnSOD protein levels were increased relative to wild-type in the long-lived *sod-2*(*ok1030*) homozygous deletion allele. Relative changes are reported in Table 2A.

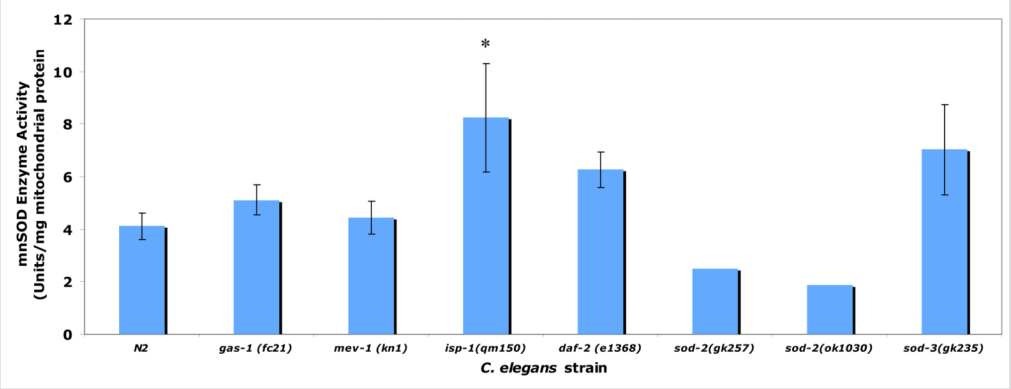

Figure 5. MnSOD enzyme activity assessment in isolated mitochondria of RC mutants

Only the complex III mutant (*isp-1*) had significantly elevated MnSOD enzyme activity in isolated mitochondria. Trends toward upregulation observed in *gas-1*, *daf-2*, and *sod-3* did not reach statistical significance, perhaps because of small sample size. No discrimination was made by this assay between protein encoded by *sod-2* or *sod-3*. Bars represent mean ± standard deviation of two to five biological replicates per strain. Single mitochondria preparations were assessed for each of the *sod*-2 knockout alleles, which demonstrated similar reductions in MnSOD activity relative to N2. *, $p < 0.05$. Percent change in each mutant strain relative to N2 is reported in Table 2A.

Table 1

***C. elegans* strain description, homology, and lifespan**

The role of *in vivo* oxidant stress on longevity was studied in three RC subunit missense mutants, three MnSOD knockout mutants, and an insulin receptor missense mutant. FUDR-based median lifespan assessment was largely consistent with previously reported lifespan findings in these strains. * indicates concurrent wild-type (N2 Bristol) control for MnSOD mutant lifespan comparison. All other strains were concurrently studied with the unmarked wild-type (N2 Bristol) control. RC, respiratory chain. Lifespan plots and animal number studied for each mutant are provided in Supplementary Figure 4.

C. elegans Strain Name	Gene Function and Human Homologue	Mutation Type	Human-Worm Protein Similarity	Lifespan (20°C)			
				Interpretation	Median	Mean	Maximum
N2 Bristol	-	wild-type	-	vs. RC Mutants vs. MnSOD mutants*	14 17	16.9 19.9	21 23
gas-1 (fc21)	Complex I subunit (*NDUFS2*)	missense	83.4%	short-lived	12	15.6	20
mev-1 (kn1)	Complex II subunit (*SDH-C*)	missense	75.3%	unchanged	14	16.4	22
isp-1 (qm150)	Complex III subunit (*UQCRFS1*)	missense	97.5%	long-lived	20	22.4	31
daf-2 (e1368)	Insulin receptor (*IR*)	missense	62.0%	long-lived	31	31.1	38
sod-2 (gk257)	Mitochondrial MnSOD (*SOD2*) - Cel chr. X	knockout	97.3%	long-lived*	19	20.7	24
sod-2 (ok1030)	Mitochondrial MnSOD (*SOD2*) - Cel chr. X	knockout	97.3%	long-lived*	20	21.6	25
sod-3 (gk235)	Mitochondrial MnSOD (*SOD2*) - Cel chr. I	knockout	97.2%	long-lived*	18.5	20.0	23

Mitochondrion. Author manuscript; available in PMC 2013 April 29.

Table 2

Multi-dimensional summary of relative alterations in lifespan, oxidant levels, oxidant scavenging, and oxidant damage in *C. elegans* mitochondrial respiratory chain mutants

A) Relative steady-state oxidant burden (assessed by MitoSOX PB fluorescence), mitochondria membrane potential ($\Delta\Psi_m$, assessed by TMRE PB fluorescence) and antioxidant defenses in synchronous young adult stage animals of each strain compared to wild-type nematodes under non-stressed conditions. Red dotted line separates *in vivo* (above line) from *in vitro* (below line) parameters. Black arrows indicate direction of change relative to wild-type, where % and X indicate percent change below and above two-fold, respectively. $O^{\bullet}$ indicates oxidant levels primarily in the form of superoxide, as well as its site of production in the mitochondria matrix via complex I and predominantly into the intermembrane space via complex III. *, results are provided for *sod-2*(*gk257*), which was the main *sod-2* allele analyzed in most assays. **, 8% increase (essentially no change) was observed by MnSOD Western for *sod-2*(*gk257*) mitochondria, while a 3-fold increased MnSOD protein level was observed for *sod-2*(*ok1030*) (Figure 4C). These allelic differences may relate to the binding site of the antibody within the protein, rather than reflecting increased intact protein. **B)** Relative oxidant levels and MnSOD transcriptional response in two paralagous MnSOD mutants following 24 hour oxidant stress (1 mM paraquat exposure) relative to wild-type in young adult stage animals. *In vivo* oxidant levels following oxidative stress increase to the greatest extent in the complex I mutant (*gas-1*, 55% increased MitoSOX PB fluorescence) and to a lesser extent in the complex II mutant (*mev-1*, 21% increased MitoSOX PB fluorescence) and complex III mutant (*isp-1*, 8.3% increased MitoSOX PB fluorescence). Increased *in vivo* oxidant burden occurred despite marginally increased *sod-2* expression (below a 2-fold level

of induction) and significant *sod-3* induction (greater than 5-fold level of induction) in all three respiratory chain (RC) mutants.

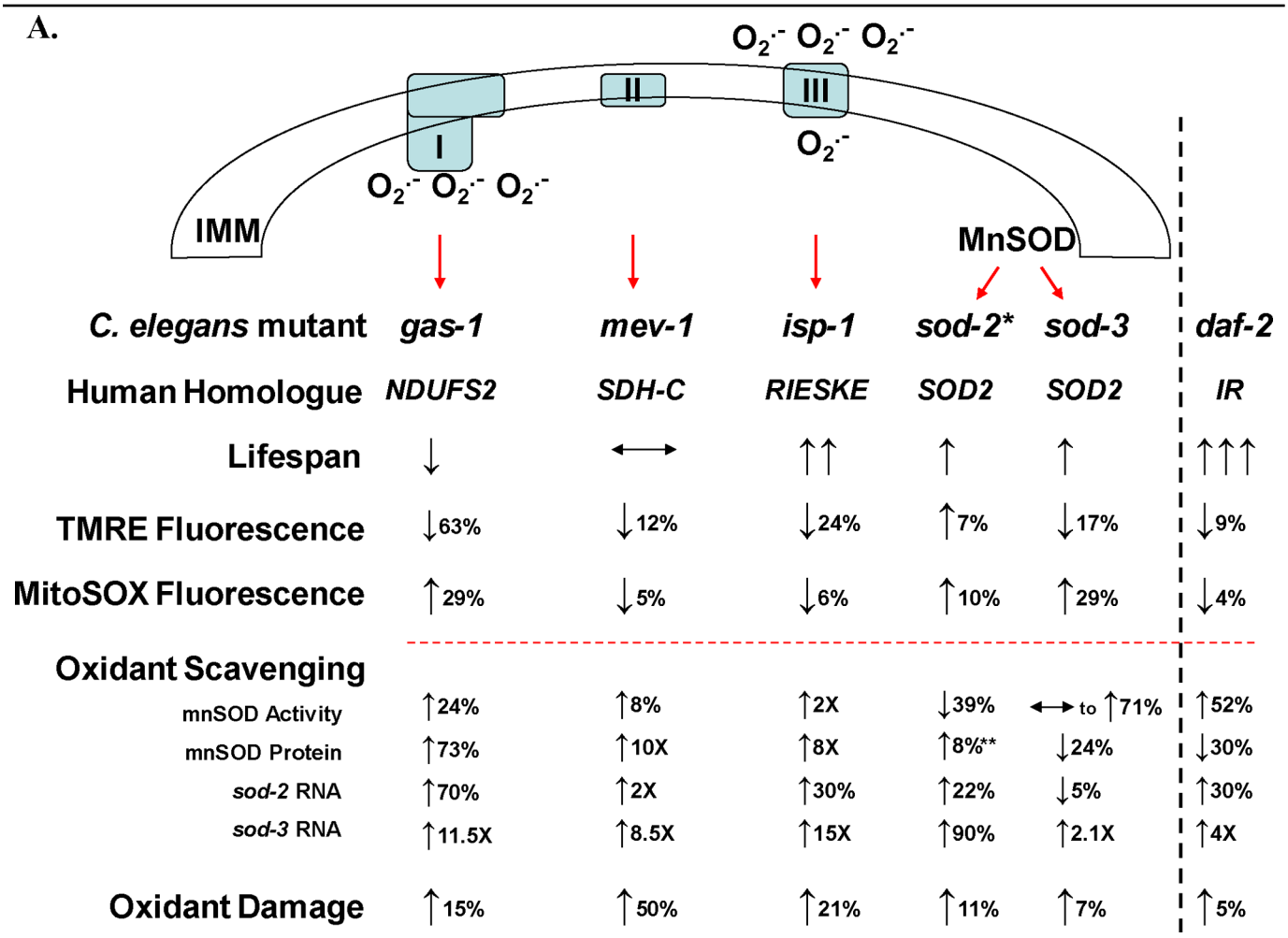

B.

C. elegans Strain	OXIDANT LEVEL	OXIDANT SCAVENGING	
	PB Fluorescence (MitoSOX)	*sod-2* Relative Expression	*sod-3* Relative Expression
gas-1(fc21)	↑ (55%)	↑ (84%)	↑ (7.4 X)
mev-1(kn1)	↑ (21%)	↑ (30%)	↑ (5.6 X)
isp-1(qm150)	↑ (8.3%)	↑ (40%)	↑ (9.1 X)
daf-2(e1368)	↓ (7.2%)	↑ (23%)	↑ (20%)
sod-2(gk257)	↓ (1.2%)	↓ (65%)	↓ (7%)
sod-3(gk235)	↑ (16%)	↓ (30%)	↓ (13%)